NANO LETTERS

Inorganic Electrochromic Metasurface in the Visible

Yohan Lee,* Jonas Herbig, Serkan Arslan, Dominik Ludescher, Monika Ubl, Andreas Georg,
Mario Hentschel, and Harald Giessen*

Cite This: https://doi.org/10.1021/acs.nanolett.5c01396

Read Online

ACCESS | Metrics & More | Article Recommendations | Supporting Information

ABSTRACT: Color printing based on metallic or dielectric nanostructures has revolutionized color science due to its unprecedented subwavelength resolution. Evidently, the evolution toward the active control of such structural colors with smart materials is in progress for real applications. Here we experimentally demonstrate a large color gamut with high intensity and purity, as well as switching on and off based solely on tungsten trioxide (WO_3) cylindrical resonators. The strong resonances in the visible spectral range in these WO_3 metasurfaces can be reversibly switched on and off due to its electrochromism by applying alternating voltages of +2.0 V and −0.3 V. Our approach opens up possibilities for the functional diversification of commercial smart windows, as well as the development of new display technologies in the future.

KEYWORDS: Inorganic, Electrochromic, Metasurfaces, Electrically switchable, Full color switching
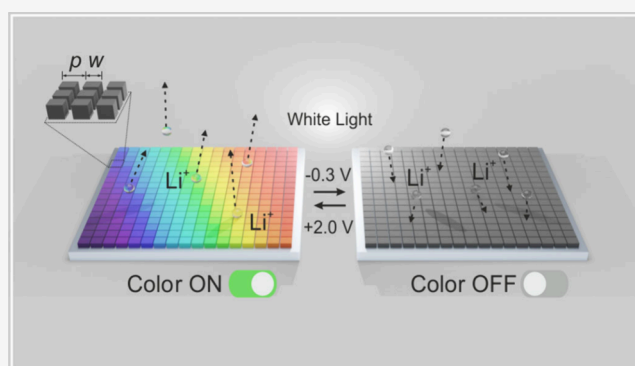
Color generation with nanostructures[1,2] has been explored since ancient times in human history, as seen in the well-known Lycurgus Cup, stained glass, and pottery.[3] Different from applying dyes or pigments as traditional techniques to generate colors, structural coloration can offer promising opportunities such as vivid and vibrant colors, high durability, precise color tuning capabilities, and environmental friendliness. Consequently, in the past decade, there have been extensive efforts employing plasmonic nanostructures toward expanding the color space and achieving high resolution and saturation, because the resonance can be easily tuned by the structural information including the size, shape, and arrangement of the nanoscatterers with recent advancement in nanofabrication and optical characterization techniques.[1] However, due to the inherent loss of metals in the visible range, the resonance peaks from plasmonic nanostructures are typically broad and less intense, preventing them from truly competing with the color space of traditional pigments.[4−9] In this context, high-index dielectric nanostructures such as silicon (Si) or titanium dioxide (TiO_2) have garnered significant attention for nanoscale color printing, because they can support optical resonances in the visible spectrum through Mie resonances.[10−15] Such materials possess enhanced resonance quality factors related to the saturation of colors due to absorption losses.

The notable advantage achievable only through structural color reproduction is the ability to actively control the color via external stimuli, which is not possible with traditional methods. The realization of such a dynamic structural color is crucial for extending functionality beyond merely static images to include

animations. Commonly reported approaches involve employing active materials that respond to physical or chemical principles to alter the refractive index or size of nanoresonators,[16−24] or to change the refractive index of the background of nanostructures.[25−32] Previous studies on dynamic structural colors have two main limitations: (1) Most studies have focused on transitions to different colors rather than ON/OFF color switching.[19−27,30,31] For real applications, it is essential to have several basic colors (such as red, green, and blue) that can be turned on and off, along with their combinations, similar to the principle of commercialized displays. (2) The materials used for color reproduction and the active materials used for color control are different.[28,29,32,33] Adding other types of materials for active control could introduce compatibility issues or compromise the desired optical properties, potentially reducing the overall efficiency or reliability of the color-changing process.

Here, we introduce an electrically switchable full-color palette made from tungsten trioxide (WO_3) nanostructures based on an electrochemically driven tuning of its refractive index. The proposed platform consisting of solely one material is able to
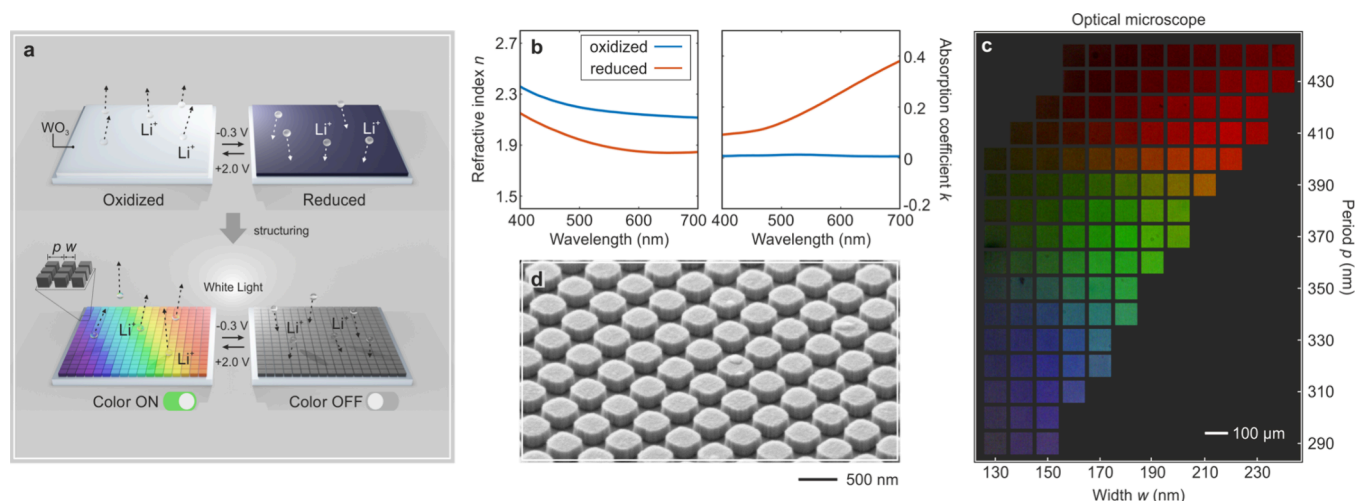
Figure 1. Concept of full-color-switchable metasurfaces made from tungsten trioxide (WO_3). (a) Schematic of the working principle of the inorganic electrochromic metasurfaces. WO_3 as a thin film shows a simple electrochromic property from transparent to deep blue with electrochemical redox reaction (top). Nanopatterned WO_3 not only allows for the generation of a wide color gamut depending on the period (p) and width (w) of nanoresonators but also allows the colors to be switched on and off at a faster rate (bottom). (b) Refractive index (left) and absorption coefficient (right) of WO_3 at oxidized and reduced states. WO_3 has a relatively high refractive index ($n \approx 2.2$) in the visible. Evidently, nearly no absorption is observed at the oxidized state in the visible, while electrochemically reduced WO_3 shows dispersive absorption. (c) Optical microscopy image with 5× objective of the color palette made from WO_3 metasurfaces with the combinations of different p and w. (d) Scanning electron microscopy (SEM) image showing the WO_3 metasurface with one specific condition of p and w.

express a wide color gamut, as well as to dynamically switch on and off via an applied voltage.

The concept of our inorganic metasurfaces is illustrated in Figure 1. Pristine WO_3, utilized in current smart windows, is transparent in its as-deposited film state (top of Figure 1a). The dynamic behavior of WO_3 is enabled by the unique phenomenon of the material changing color in response to an electric stimulus, known as electrochromism. Depending on the electrochemical reactions induced by the intercalation or deintercalation of lithium ions dissolved in an electrolyte, it can exhibit a switch from transparent to a deep blue color (see Figure S1 in the Supporting Information). This switching mechanism takes place by the following reaction:[34]

$$WO_3 + xLi^+ + xe^- \rightleftharpoons Li_xW_x^{5+}W_{1-x}^{6+}O_3$$
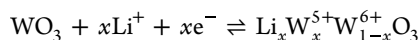
In this work, we find that nanopatterned WO_3 can express a wide range of color space with high purity by tailoring the geometric conditions of the patterns, such as period p and width w (bottom of Figure 1a). Furthermore, leveraging the electrochromic phenomenon of the material itself, the brilliant colors can be switched off and on again by applying voltages of −0.3 V and +2.0 V (versus a reference electrode). The proposed concept shows the novelty that color generation and switching are simultaneously achieved solely with monolithic WO_3.

The mechanism of our active metasurfaces relies on the variation of the refractive index of WO_3 by applied voltages. Figure 1b depicts the real and imaginary parts of the refractive indices of WO_3 in its oxidized (or pristine) and reduced states (see Table S1 in the Supporting Information for detailed values). These data explain why WO_3 appears deep blue when electrochemically reduced. It is because the absorption in the longer wavelength range of the visible spectrum is higher than that in the shorter wavelength range. We notice that in the visible, WO_3 has a relatively high refractive index (around 2.2) and exhibits nearly no intrinsic losses when oxidized, enabling it to support a high-Q resonance. Although it cannot support strong Mie resonance in a single nanoparticle due to its refractive

index being lower than 3.5 in the visible range, unlike silicon or gallium arsenide, it can exhibit lattice resonance by controlling the interactions between the scatterers through periodic arrangement. Notably, as WO_3 gets electrochemically reduced by an external voltage, the absorption coefficient of WO_3 (the imaginary part of the refractive index) increases, thereby enabling the suppression of such a resonance.

In Figure 1c, we display the color palette generated by our WO_3 metasurfaces. Optical images of the colors are taken with a 5× NA 0.15 objective at a fully closed aperture stop in order to collect only components near normal incidence. (Angle dependency of the metasurfaces is presented in Figure S2 in the Supporting Information.) It is clear that the colors and their intensities are determined by the period p and width w of the WO_3 nanoresonators. Figure 1d depicts a scanning electron microscopy (SEM) image of our WO_3 metasurface taken for one of the structures that have different p and w. The nanopattern is a cuboid shape as designed, which shows an excellent quality of nanofabrication. Additional SEM images of the structures with various conditions can be found in Figure S3 in the Supporting Information. The details of nanofabrication are provided in Methods and Figure S4 in the Supporting Information.

The switching performance of our WO_3 metasurfaces is investigated in Figure 2. The resonators are switched between ON and OFF states at applied voltages of +2.0 V and −0.3 V while tracking the transmitted intensity (see Methods for the detail). In Figure 2a, the modulated transmitted intensity is depicted in the top graph, corresponding to the voltage applied to the WO_3 nanopatterns shown in the bottom graph. When a negative voltage is applied to the electrode, the cations present in the electrolyte are attracted to the WO_3 surface. These ions then undergo intercalation into the WO_3. This process occurs primarily through electrostatic interactions, where the ions are inserted into specific sites within the WO_3, resulting in a rapid reduction of the light intensity. After intercalation, the ions diffuse further into WO_3. This diffusion occurs due to the concentration gradient of ions within the WO_3, where the ions
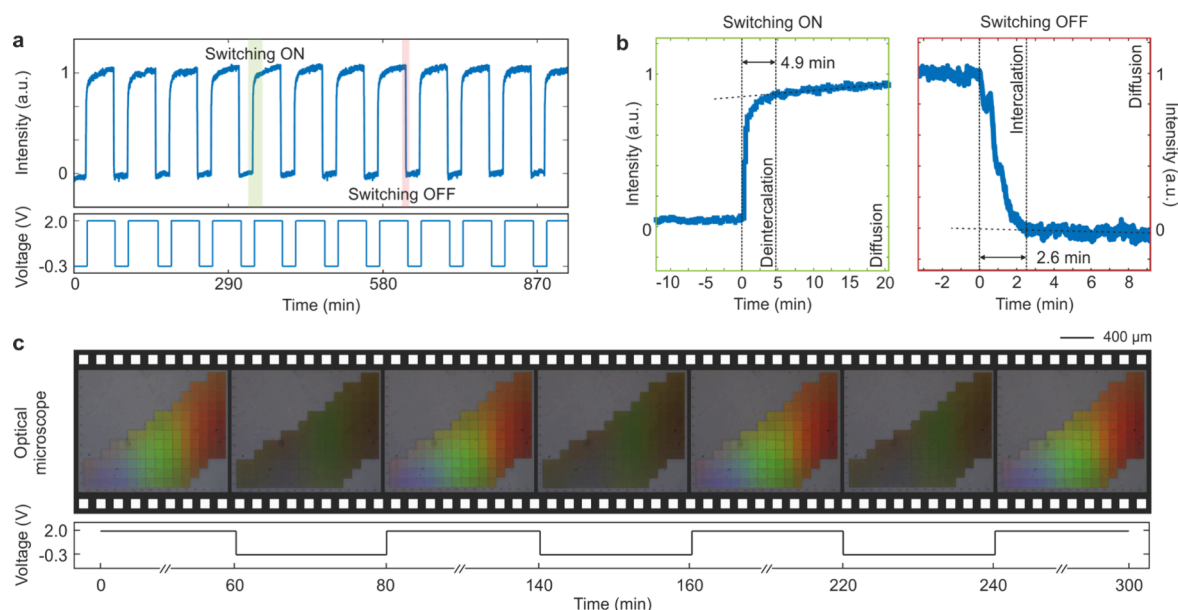
Figure 2. Switching performance by electrical stimulation of WO_3 metasurfaces. (a) Transmitted intensity through the WO_3 metasurface cycling between the ON and OFF states (top). The green area depicts the switching ON window, while the red area represents the switching OFF window. The voltage range is set between +2.0 and −0.3 V (bottom). (b) Plots corresponding to the switching ON and OFF states, as indicated in panel a. The cation intercalation/deintercalation and diffusion regions are distinguished based on the point where the rate of change in intensity converges (indicated by the dashed line). The time required for cation deintercalation (left) and intercalation (right) is presented. (c) Optical microscopy images showing several cycles of colors switching ON and OFF when the applied voltage is cycled in situ between +2.0 V for 60 min to −0.3 V for 20 min.

tend to move toward regions of lower concentration. Similarly, when a voltage is applied in the opposite direction to the electrode, deintercalation occurs first, followed by diffusion, resulting in recovery of light intensity. Twelve switching cycles are illustrated with a period of 80 min (20 min for OFF and 60 min for ON), confirming full switching between ON and OFF states without noticeable degradation. Although further switching is limited by the rapid evaporation of the electrolyte, experimental studies have reported that the switching stability of WO_3 is maintained even after more than 100 cycles at the laboratory scale.[34,35]

Figure 2b displays the analysis of the switching time from ON to OFF (left) and from OFF to ON (right). The onset of diffusion is defined as the point at which the rate of change in the light intensity becomes constant. The difference in the speed between intercalation and diffusion primarily arises from their distinct governing mechanisms. Intercalation occurs rapidly at the electrode−electrolyte interface, driven by charge transfer and electrostatic interactions, whereas diffusion is a bulk process that is limited by the energy barrier within the electrode lattice. The slower diffusion process results from the need for ions to migrate through the solid structure, which is constrained by concentration gradients and material properties, such as ionic diffusivity and lattice openness. We focused on the time required for cation intercalation/deintercalation, as most of the light intensity change occurs during this process rather than during the diffusion process. We obtain the deintercalation time of 4.9 min and the intercalation time of 2.6 min. Intercalation occurs more rapidly, as ions are readily inserted into available sites, driven by electrostatic attraction. In contrast, deintercalation is slower due to stronger Coulombic interactions and structural distortions, which increase the energy barrier for ion extraction. It is worth mentioning that the color switching speed during the electrochemical reaction can be affected by several key factors, including the thickness of WO_3, the cation concentration in an

electrolyte, and the substrate temperature. In this work, acetonitrile containing 100 mM $LiClO_4$ as an electrolyte and room temperature are employed in all of the demonstrations. Acetonitrile is widely utilized in lithium-ion batteries, electrochemical sensors, and high-speed energy storage systems due to its wide electrochemical stability window, high ionic conductivity, and low viscosity. More detailed data on switching speed can be found in Figure S5 in the Supporting Information. Also, the thickness of WO_3 is fixed at 200 nm, which directly affects the support of the lattice resonance. Details regarding the resonance intensity as a function of thickness can be found in Figure S6 in the Supporting Information. To improve the switching speed, an electrolyte such as sulfuric acid, which contains smaller H^+ ions instead of Li^+ ions, can be considered. Additionally, since the stoichiometry of WO_3 deposited by sputtering significantly affects the switching characteristics, optimizing parameters such as the oxygen concentration during sputtering is essential.

To visualize the switching performance of our metasurfaces, the images with a 5× objective are depicted in Figure 2c. Furthermore, movies that record the color dynamics of the palette are presented in Supporting Information Movie 1 (for switching OFF) and Movie 2 (for switching ON). The colors generated by WO_3 metasurfaces at a pristine state can be switched off upon lithium ion intercalation induced by an applied voltage of −0.3 V. Importantly, the colors of the palette can be nicely restored with a voltage of +2.0 V. This indicates that the Li_xWO_3 is converted back to WO_3, therefore displaying brilliant colors again. Such reversible switching is of great importance for dynamic applications.

Color ON/OFF switching via external voltages is carried out in a liquid electrolyte by using an electrochemical cell with a three-electrode system (Figure 3a; see Methods). For both ON and OFF cases, the spectral analysis of the representative colors among various structural information (period p and width w) is
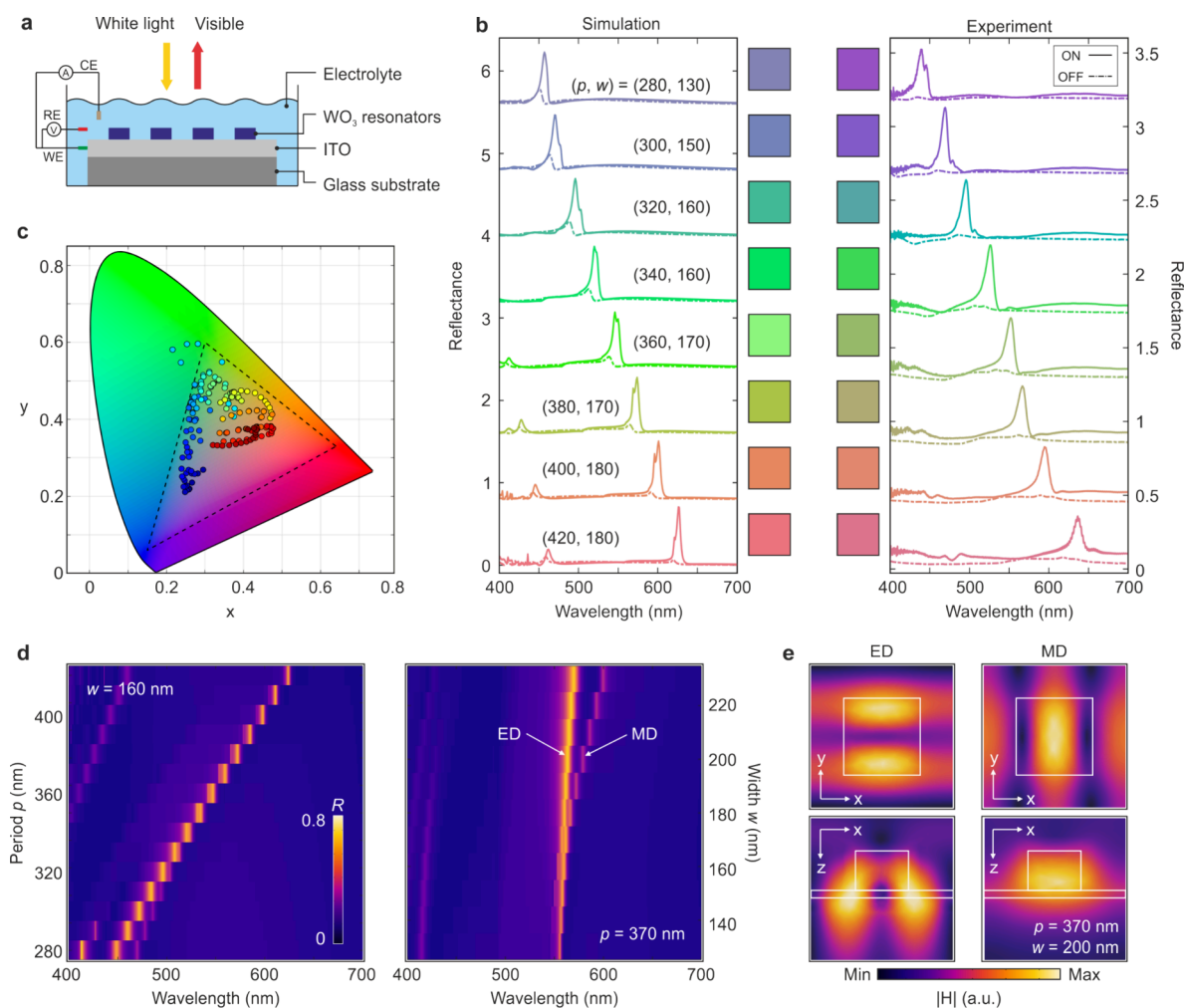
C

Figure 3. Optical characterization of the colors from WO$_3$ metasurfaces. (a) Schematic of the electrochemical cell (three-electrode setup). The WO$_3$ metasurface immersed in the electrolyte is illuminated by a white light source with normal incidence, and the reflected light is captured by an objective. (b) Simulated and experimental normal reflectance spectra for the ON and OFF states. Each plot has been offset by a constant value for clarity, allowing for the comparison of different data sets. For the ON state, the colors corresponding to the reflectance spectra are depicted in the adjacent squares. (c) Measured reflectance spectra plotted in CIE 1931 color map. A large color gamut is obtained by varying the parameters of the metasurfaces (period p and width w). The triangle formed by the dashed lines in the plot represents the standard RGB (sRGB) color space. (d) Simulated reflectance spectra as a function of wavelength for different periods or widths. (Left) With the width fixed to 160 nm, high reflectance with narrow bandwidth is mainly dependent on the period of nanostructures. (Right) Electric dipole (ED) and magnetic dipole (MD) resonances are observed depending on the widths with the period fixed to 370 nm. (e) The magnetic field distributions of the cross sections at the ED and MD resonances, respectively, in WO$_3$ resonators with $p = 370$ nm and $w = 200$ nm.

carried out and presented in Figure 3b. The simulated spectra (left panel) indicate that the reflectance resonance has a high peak (around 70%) with a narrow bandwidth, resulting in a high purity color. Notably, the remaining reflectance which is slightly blue-shifted can be seen even in the OFF state. It can be visually observed during the color change in Figure 2c (the colors are not completely "OFF", and become slightly different). This is because our mechanism of ON/OFF switching is based on electrochromism of WO$_3$, which is absorption tuning by electrical stimulus. The absorption coefficient of WO$_3$ increased by electrochemical reduction is not sufficiently high to suppress the entire reflected intensity. The experimental reflectance spectra and their colors (right panel) show an overall good agreement with respect to the simulation results. However, it can be observed that the peak value of the reflectance is lower in the experimental cases, which is due to the fact that the simulation did not account for the absorption by the electrolyte. From measured reflectance spectra, the structural colors that can be

expressed through the combination of p and w of WO$_3$ metasurfaces are displayed in the CIE 1931 color space (Figure 3c).

To elucidate the underlying physics of the observed spectral characteristics, we numerically calculated the reflectance while varying p and w, respectively (Figure 3d). Above all, the reflectance peak clearly exhibits red-shifts with increasing period p (left panel), meaning the colors from our metasurfaces are mainly based on lattice resonance.[36] Also, we can observe the typical characteristics where the dipole resonance shifts according to the structural parameter w of the scatterers (right panel). Figure 3e depicts the magnetic field distribution of the cross-section at the resonant peaks with $p = 370$ nm and $w = 200$ nm. Figure 3e enables the differentiation of various types of dipole resonance. In magnetic dipole (MD) resonance, the H-field forms a toroidal (looped) pattern inside the particle, indicating a circulating current loop with the strongest field concentrated at the center. In contrast, electric dipole (ED)
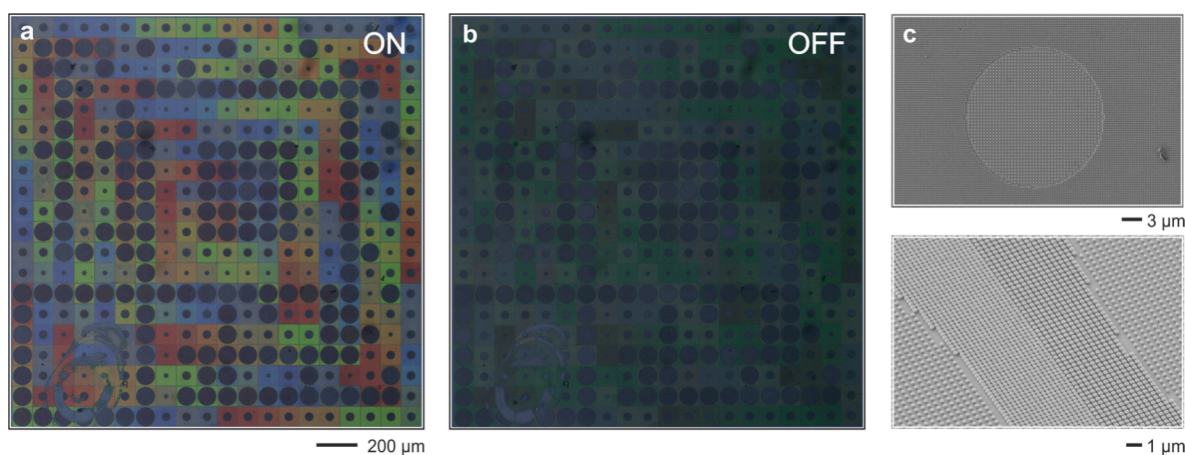
Figure 4. Dynamic color switching of arbitrary image. (a) Optical microscopy image of the modified artwork, inspired by "Orion Gris" of Victor Vasarely. Nanopatterned WO_3 is in the ON state in the electrochemically oxidized state. The size of whole pattern is 2 mm by 2 mm. (b) The artwork in OFF state during electrochemically reduced reaction for color switching. (c) Enlarged SEM images of fabricated sample (Top: one square building block including a circle, Bottom: the edge between building blocks).

resonance shows a more symmetric, noncirculating *H*-field distribution, with the strongest field near the particle surface. MD resonance is driven by internal current loops, while the ED resonance follows the oscillation of the incident electric field. In principle, each WO_3 nanocuboid can support a Mie resonance due to its relatively high refractive index. However, its refractive index is not sufficiently high to be excited in a single resonator like silicon. In this sense, we arrange WO_3 scatterers into periodic metasurfaces to enhance the reflectance efficiency due to the coupling effect between dipole resonances, and to suppress the other high-order resonant modes as a photonic band gap.[13,37]

WO_3 metasurfaces have the potential to go beyond the light and thermal energy blocking capabilities of conventional smart windows,[38] enabling the reproduction of arbitrary color images and their ON/OFF switching. To demonstrate this ability, we proposed a millimeter-sized artwork as a blueprint inspired by Victor Vasarely's *Orion Gris* (Figure 4a). The basic structure is a square shape containing a circle in the center. Each structure has circles of different sizes and backgrounds of different colors. Figure 4b represents the image erased into the OFF state for dynamic switching. The SEM images of the basic structure and edge area are shown in Figure 4c. It is worth mentioning that those SEM images were taken from the sample that already got switched on and off several times. This means that WO_3 nanopatterns still exhibit no noticeable degradation during lithium ion intercalation and deintercalation within a safe voltage range.

In summary, we have introduced novel active metasurfaces that operate in the visible spectrum. The high refractive index and electrochromic property of WO_3 enable a high-purity color gamut with an unprecedented subwavelength resolution and dynamic ON/OFF switching via applied voltages. Structural engineering and optimization of the electrochemical environment can be carried out to further improve the switching speed and larger color space for real world applications. Our concept will be of importance for solid-state devices with electrically tunable optical responses and reflective displays, especially once the engineering task of addressing single pixels has been solved.[39,40]

■ METHODS

Structure Fabrication and Characterization. As substrate, we used ITO (50 nm) coated glass to operate the ON/OFF switching of reflected colors and allow electrical addressability. A 200 nm layer of WO_3 was deposited onto the substrate using reactive DC-magnetron sputtering (Star 100-TetraCo) with a metallic tungsten target. The deposition was performed with a power of 0.58 kW, a pressure of 1.1×10^{-2} mbar, an Ar flow rate of 200 sccm, and an O_2 flow rate of 70 sccm. The substrate was not heated, and its temperature during deposition was below 100 °C. The film was covered with a double-layered poly(methyl-methacrylate) (PMMA) positive tone resist (Allresist AR-P 642.06 200K, Allresist AR-P 672.02 950K), used to define nanostructures with electron beam lithography (EBL). After development in methylisobutylketone (MIBK), we used electron-gun evaporation to deposit a 30 nm chromium (Cr) layer. After lift-off, Cr served as hard-mask for the subsequent chemical etching process, which removed uncovered WO_3. The WO_3 film was etched in a PlasmaPro80 etcher from Oxford with 100 W of radio frequency power with an atmosphere of 10 sccm of N_2, 15 sccm of CF_4, and 10 sccm of SF_6. As a result, we obtained a WO_3 metasurface after removing Cr via a commercial Cr remover. Scanning electron microscopy images were taken with a Zeiss SEM Gemini 560.

Spectral Measurements. The presented reflectance spectra were measured in a setup based on an upright optical microscope (Nikon Eclipse LV). The exit path of the microscope was connected to the entrance slit of a Princeton Instruments grating spectrometer (Iso plane 160) with a Peltier-cooled CCD camera (PIXIS 256). The sample was placed on a motorized XY stage (Märzhäuser) and illuminated through the objective (Nikon TU Plan ELWD 20×, NA 0.4) by the built-in halogen white light lamp. We ultilized internal apertures of the microscope to restrict the image plane (field stop) to the 200 μm by 200 μm WO_3 metasurface arrays. Additionally, the aperture in the microscope Fourier plane (aperture stop) was closed to restrict incident and collected light to angles close to normal incidence, blocking light scattered from the surrounding substrate. The measured spectra were normalized to the reflectance of a protected aluminum mirror (Thorlabs).

Numerical Simulations. Numerical simulations were carried out using the commercial software COMSOL Multi-

physics based on a finite element method. Periodic boundary conditions were used for the calculation of the structure arrays. The refractive index of SiO_2 was taken as 1.47.

Electrochemical Switching of Metasurfaces. We utilized a custom-built electrochemical cell to electrically switch the WO_3 metasurfaces using a three-electrode configuration. The cell was sealed with a thin glass window at the top and bottom to allow optical access during reflectance/transmittance experiments. It included side ports for electrolyte inflow and outflow as well as connections for the reference and counter electrode. ITO (for electrical contact) underneath the WO_3 nanopatterns served directly as the working electrode. The counter electrode was a platinum wire, and the reference electrode was silver/silver choride (Ag/AgCl), both in contact with 100 mM $LiClO_4$ electrolyte. A potentiostat (BioLogic SP-200) regulated the voltage over time. Temporal and switching characteristics were analyzed using a 633 nm He−Ne laser and a photodiode.

■ ASSOCIATED CONTENT

Ⓢ Supporting Information

The Supporting Information is available free of charge at https://pubs.acs.org/doi/10.1021/acs.nanolett.5c01396.

> Photograph of the WO_3 thin films in different electrochemical states, along with additional simulation results on the angle dependence and thickness-dependent reflectance spectra of the proposed metasurfaces; fabrication procedure of the WO_3 metasurfaces, followed by a plot illustrating the switching speed measurement; table summarizing the measured complex refractive indices of WO_3 under the different electrochemical conditions (PDF)
> Movie 1: color dynamics of the palette for switching OFF (MP4)
> Movie 2: color dynamics of the palette for switching ON (MP4)

■ AUTHOR INFORMATION

Corresponding Authors

Yohan Lee − *4th Physics Institute and Research Center SCoPE, University of Stuttgart, 70569 Stuttgart, Germany;* ⓞ orcid.org/0000-0002-6809-3210; Email: y.lee@pi4.uni-stuttgart.de

Harald Giessen − *4th Physics Institute and Research Center SCoPE, University of Stuttgart, 70569 Stuttgart, Germany;* Email: giessen@pi4.uni-stuttgart.de

Authors

Jonas Herbig − *4th Physics Institute and Research Center SCoPE, University of Stuttgart, 70569 Stuttgart, Germany*

Serkan Arslan − *4th Physics Institute and Research Center SCoPE, University of Stuttgart, 70569 Stuttgart, Germany*

Dominik Ludescher − *4th Physics Institute and Research Center SCoPE, University of Stuttgart, 70569 Stuttgart, Germany*

Monika Ubl − *4th Physics Institute and Research Center SCoPE, University of Stuttgart, 70569 Stuttgart, Germany*

Andreas Georg − *Fraunhofer Institute for Solar Energy Systems, 79110 Freiburg, Germany*

Mario Hentschel − *4th Physics Institute and Research Center SCoPE, University of Stuttgart, 70569 Stuttgart, Germany*

Complete contact information is available at: https://pubs.acs.org/10.1021/acs.nanolett.5c01396

Author Contributions

Y.L conceived the original idea. Y.L., M.H., and H.G. supervised the work. Y.L. performed simulations and modeling for the WO_3 nanopatterns. A.G. provided WO_3 films. Y.L., M.U., and M.H. fabricated and characterized the samples. Y.L., J.H., and D.L. measured the color samples. S.A. performed the spectroscopic measurements. All authors participated in the preparation and writing of the manuscript.

Notes

The authors declare no competing financial interest.

■ ACKNOWLEDGMENTS

■ REFERENCES

(1) Kelly, K. L.; Coronado, E.; Zhao, L. L.; Schatz, G. C. The optical properties of metal nanoparticles: the influence of size, shape, and dielectric environment. *J. Phys. Chem. B* **2003**, *107*, 668−677.

(2) Biagioni, P.; Huang, J.-S.; Hecht, B. Nanoantennas for visible and infrared radiation. *Rep. Prog. Phys.* **2012**, *75*, 024402.

(3) Barchiesi, D. Lycurgus Cup: Inverse problem using photographs for characterization of matter. *J. Opt. Soc. Am. A* **2015**, *32*, 1544−1555.

(4) Maier, S. A.; Atwater, H. A. Plasmonics: Localization and guiding of electromagnetic energy in metal/dielectric structures. *J. Appl. Phys.* **2005**, *98*, 011101.

(5) Kumar, K.; Duan, H.; Hegde, R. S.; Koh, S. C. W.; Wei, J. N.; Yang, J. K. W. Printing colour at the optical diffraction limit. *Nat. Nanotechnol.* **2012**, *7*, 557−561.

(6) Tan, S. J.; Zhang, L.; Zhu, D.; Goh, X. M.; Wang, Y. M.; Kumar, K.; Qiu, C.-W.; Yang, J. K. W. Plasmonic color palettes for photorealistic printing with aluminum nanostructures. *Nano Lett.* **2014**, *14*, 4023−4029.

(7) Clausen, J. S.; Højlund-Nielsen, E.; Christiansen, A. B.; Yazdi, S.; Grajower, M.; Taha, H.; Levy, U.; Kristensen, A.; Mortensen, N. A. Plasmonic metasurfaces for coloration of plastic consumer products. *Nano Lett.* **2014**, *14*, 4499−4504.

(8) Knight, M. W.; King, N. S.; Liu, L.; Everitt, H. O.; Nordlander, P.; Halas, N. J. Aluminum for Plasmonics. *ACS Nano* **2014**, *8*, 834−840.

(9) Xue, J.; Zhou, Z.-K.; Wei, Z.; Su, R.; Lai, J.; Li, J.; Li, C.; Zhang, T.; Wang, X.-H. Scalable, full-colour and controllable chromotropic plasmonic printing. *Nat. Commun.* **2015**, *6*, 8906.

(10) Kuznetsov, A. I.; Miroshnichenko, A. E.; Brongersma, M. L.; Kivshar, Y. S.; Luk'yanchuk, B. Optically resonant dielectric nanostructures. *Science* **2016**, *354*, aag2472.

(11) Proust, J.; Bedu, F.; Gallas, B.; Ozerov, I.; Bonod, N. All-dielectric Colored Metasurfaces with silicon Mie resonators. *ACS Nano* **2016**, *10*, 7761−7767.

(12) Flauraud, V.; Reyes, M.; Paniagua-Domínguez, R.; Kuznetsov, A. I.; Brugger, J. Silicon nanostructures for bright field full color prints. *ACS Photon.* **2017**, *4*, 1913−1919.

(13) Sun, S.; Zhou, Z.; Zhang, C.; Gao, Y.; Duan, Z.; Xiao, S.; Song, Q. All-dielectric full-color printing with TiO_2 metasurfaces. *ACS Nano* **2017**, *11*, 4445−4452.

(14) Hentschel, M.; Koshelev, K.; Sterl, F.; Both, S.; Karst, J.; Shamsafar, L.; Weiss, T.; Kivshar, Y. S.; Giessen, H. Dielectric Mie voids: Confining light in air. *Light Sci. Appl.* **2023**, *12*, 3.

(15) Decker, M.; Staude, I.; Falkner, M.; Dominguez, J.; Neshev, D. N.; Brener, I.; Pertsch, T.; Kivshar, Y. S. High-efficiency dielectric Huygens' surfaces. *Adv. Opt. Mater.* **2015**, *3*, 813−820.

(16) Duan, X.; Kamin, S.; Liu, N. Dynamic plasmonic colour display. *Nat. Commun.* **2017**, *8*, 14606.

(17) Byers, C. P.; Zhang, H.; Swearer, D. F.; Yorulmaz, M.; Hoener, B. S.; Huang, D.; Hoggard, A.; Chang, W.-S.; Mulvaney, P.; Ringe, E.; Halas, N. J.; Nordlander, P.; Link, S.; Landes, C. F. From tunable core-shell nanoparticles to plasmonic drawbridges: Active control of nanoparticle optical properties. *Sci. Adv.* **2015**, *1*, e1500988.

(18) Tsuboi, A.; Nakamura, K.; Kobayashi, N. A localized surface plasmon resonance-based multicolor electrochromic device with electrochemically size-controlled silver nanoparticles. *Adv. Mater.* **2013**, *25*, 3197−3201.

(19) Wang, G.; Chen, X.; Liu, S.; Wong, C.; Chu, S. Mechanical chameleon through dynamic real-time plasmonic tuning. *ACS Nano* **2016**, *10*, 1788−1794.

(20) Huang, M.; Tan, A. J.; Büttner, F.; Liu, H.; Ruan, Q.; Hu, W.; Mazzoli, C.; Wilkins, S.; Duan, C.; Yang, J. K. W.; Beach, G. S. D. Voltage-gated optics and plasmonics enabled by solid-state proton pumping. *Nat. Commun.* **2019**, *10*, 5030.

(21) Li, N.; Wei, P.; Yu, L.; Ji, J.; Zhao, J.; Gao, C.; Li, Y.; Yin, Y. Dynamically switchable multicolor electrochromic films. *Small* **2019**, *15*, 1804974.

(22) Tseng, M. L.; Yang, J.; Semmlinger, M.; Zhang, C.; Nordlander, P.; Halas, N. J. Two-dimensional active tuning of an aluminum plasmonic array for full-spectrum response. *Nano Lett.* **2017**, *17*, 6034−6039.

(23) Zhang, C.; Jing, J.; Wu, Y.; Fan, Y.; Yang, W.; Wang, S.; Song, Q.; Xiao, S. Stretchable all-dielectric metasurfaces with polarization-insensitive and full-spectrum response. *ACS Nano* **2020**, *14*, 1418−1426.

(24) Liu, L.; Aleisa, R.; Zhang, Y.; Feng, J.; Zheng, Y.; Yin, Y.; Wang, W. *Angew. Chem.* **2019**, *58*, 16307−16313.

(25) Franklin, D.; Frank, R.; Wu, S.-T.; Chanda, D. Actively addressed single pixel full-colour plasmonic display. *Nat. Commun.* **2017**, *8*, 15209.

(26) Zhang, Y.; Liu, Q.; Mundoor, H.; Yuan, Y.; Smalyukh, I. I. Metal nanoparticle dispersion, alignment, and assembly in nematic liquid crystals for applications in switchable plasmonic color filters and E-polarizers. *ACS Nano* **2015**, *9*, 3097−3108.

(27) Greybush, N. J.; Charipar, K.; Geldmeier, J. A.; Bauman, S. J.; Johns, P.; Naciri, J.; Charipar, N.; Park, K.; Vaia, R. A.; Fontana, J. Dynamic plasmonic pixels. *ACS Nano* **2019**, *13*, 3875−3883.

(28) Xu, T.; Walter, E. C.; Agrawal, A.; Bohn, C.; Velmurugan, J.; Zhu, W.; Lezec, H. J.; Talin, A. A. High-contrast and fast electrochromic switching enabled by plasmonics. *Nat. Commun.* **2016**, *7*, 10479.

(29) Xiong, K.; Emilsson, G.; Maziz, A.; Yang, X.; Shao, L.; Jager, E. W. H.; Dahlin, A. B. Plasmonic metasurfaces with conjugated polymers for flexible electronic paper in color. *Adv. Mater.* **2016**, *28*, 9956−9960.

(30) Lu, W.; Jiang, N.; Wang, J. Active electrochemical plasmonic switching on polyaniline-coated gold nanocrystals. *Adv. Mater.* **2017**, *29*, 1604862.

(31) Peng, J.; Jeong, H.-H.; Lin, Q.; Cormier, S.; Liang, H.-L.; De Volder, M. F. L.; Vignolini, S.; Baumberg, J. J. Scalable electrochromic nanopixels using plasmonics. *Sci. Adv.* **2019**, *5*, eaaw2205.

(32) Lin, Y.; Zheng, G.; Xin, Q.; Yuan, Q.; Zhao, Y.; Wang, S.; Wang, Z.-L.; Zhu, S.-N.; Jiang, C.; Song, A. Electrically switchable and flexible color displays based on all-dielectric nanogratings. *ACS Appl. Nano Mater.* **2021**, *4*, 7182−7190.

(33) Doshi, S.; Ji, A.; Mahdi, A. I.; Keene, S. T.; Selvin, S. P.; Lalanne, P.; Appel, E. A.; Melosh, N. A.; Brongersma, M. L. Electrochemically mutable soft metasurfaces. *Nat. Mater.* **2025**, *24*, 205−211.

(34) Lee, Y.; Yun, J.; Seo, M.; Kim, S.-J.; Oh, J.; Kang, C. M.; Sun, H.-J.; Chung, T. D.; Lee, B. Full-color-tunable nanophotonic device using electrochromic tungsten trioxide thin film. *Nano Lett.* **2020**, *20*, 6084−6090.

(35) Zheng, M.; Tang, H.; Hu, Q.; Zheng, S.; Li, L.; Xu, J.; Pang, H. Tungsten-based materials for lithium-ion batteries. *Adv. Funct. Mater.* **2018**, *28*, 1707500.

(36) Castellanos, G. W.; Bai, P.; Rivas, J. G. Lattice resonances in dielectric metasurfaces. *J. Appl. Phys.* **2019**, *125*, 213105.

(37) Babicheva, V. E.; Evlyukhin, A. B. Resonant lattice Kerker effect in metasurfaces with electric and magnetic optical responses. *Laser Photonics Rev.* **2017**, *11*, 1700132.

(38) Granqvist, C. G. Electrochromism and smart window design. *Solid State Ion.* **1992**, *53−56*, 479−489.

(39) Jung, C.; Lee, E.; Rho, J. The rise of electrically tunable metasurfaces. *Sci. Adv.* **2024**, *10*, eado8964.

(40) Jeon, N.; Noh, J.; Jung, C.; Rho, J. Electrically tunable metasurfaces: From direct to indirect mechanisms. *New J. Phys.* **2022**, *24*, 075001.